Journal of Southeast University (English Edition) Vol. 34, No. 3, pp. 408 - 414 Sept. 2018 ISSN 1003—7985

Syntheses and calculation of (E)-4-chloro-4'-ethoxystilbene and (E)-4, 4'-dichlorostilbene

Cheng Jinjin Ge Yuhua

(College of Chemistry and Chemical Engineering, Southeast University, Nanjing 210096, China)

Abstract: (E)-4-chloro-4'-ethoxystilbene (2a) and (E)-4, 4'-dichlorostilbene (2b) were synthesized by the Witting-Horner reaction. The crystals of 2a and 2b were prepared through solvent evaporation and characterized by the single-crystal X-ray diffraction. Molecular structure analysis confirms the E-configuration of C═C bond. The crystal of 2a reveals an orthorhombic and space group Pna21 structure while 2b shows a monoclinic and space group P21/c structure. The electronic structures of 2a and 2b were optimized at B3LYP/6-311 + + G (d, p) level. The Hirshfeld surface and fingerprint plot indicate close O—H and Cl—H contacts and π—π stacking in 2a and 2b. Molecular electrostatic potential shows that the O and Cl atoms of 2a and Cl atoms of 2b have the minimum energies and they are more likely to be attacked by electrophiles in reaction. Frontier molecular orbitals analysis demonstrates that the $\Delta E_{\text{LUMO-HOMO}}$ of 2a and 2b are 3.85 and 3.91 eV, respectively.

Key words: 1, 2-diphenylethylene; crystal structure; density functional theory; synthesis

DOI: 10.3969/j.issn.1003 - 7985.2018.03.018

1, 2-Diphenylethylene possesses special biological activity and interesting fluorescence property, which can be widely used in both pharmaceutical and material chemistry applications. For example, trans-3, 4, 5-trihydroxystilbene is of potent antioxidant effect, which can be used for anticancer, anti-arteriosclerosis and reducing blood fat[1-2]. Some other 1, 2-diphenylethylene derivatives were universally applied as organic optical storage materials, molecular switch materials, photon laser scanning microscopy, and fluorescent dye[3-4]. Therefore, the investigation of these compounds attracted considerable research attention. They can be prepared by the Perkin reaction, Knoevenagel reaction[5] and so on. However, most of these methods present problems such as poor steroselectivity and strict reaction conditions. Therefore, the development of convenient and efficient methods is of great interest to chemists. We decided to employ the Witting-Horner reaction for this purpose. First of all, the reaction is stereoselective and favors the E-configuration in stilbene products. In addition, the conditions of the reaction are moderate and vigorous exclusion of oxygen and moisture is not necessary. Moreover, the yield is relatively higher. We would also like to explore the structure and properties of E-stilbenes through theoretical calculations. Information about charge transfer and structure properties are obtained by the Mulliken charge distribution and Frontier molecular orbital. The reactivity of the compounds can be measured by the electrostatic potential. In summary, the overall research can be of great value in the synthesis and structural studies of E-stilbenes.

Received 2017-12-31, **Revised** 2018-02-10.

Biographies: Cheng Jinjin (1991—), female, graduate; Ge Yuhua (corresponding author), male, doctor, professor, 101004698@seu.edu.cn.

Citation: Cheng Jinjin, Ge Yuhua. Synthesesand calculation of (E)-4-chloro-4'-ethoxystilbene and (E)-4, 4'-dichlorostilbene[J]. Journal of Southeast University (English Edition), 2018, 34(3): 408 - 41. DOI: 10.3969/j.issn.1003 - 7985.2018.03.018.

1 Experimental

1.1 Materials and measurements

All reagents were purchased from Aldrich Chemical Co. and were used without further purification. The ^{1}H NMR spectra were recorded at 303 K on a Bruker Avance 400 MHz NMR spectrometer using DMSO-d_6 as solvent and TMS as an internal standard. The UV-vis absorption spectra were recorded on a Shimadzu UV-3600 spectrometer.

1.2 Procedure of preparation

The mixture of benzyl chloride (100 mmol) and triethoxyphosphine (150 mmol) was stirred at 140 ℃ for 8 h and the product diethyl benzylphosphonate was purified through vacuum distillation. A solution of diethyl benzylphosphonate (10.0 mmol) in anhrdrous tetrahydrofuran (30 mL) was stirred under nitrogen atmosphere for 0.5 h at 0 ℃ and 60% NaH (15.0 mmol) was added portionwise. Benzaldehyde (1a or 1b, 7.5 mmol) was added dropwise into the solution and the reaction mixture was stirred for 2 to 3 h at 0 ℃[6-7]. The reaction mixture was poured into cold water (150 mL) to precipitate the product. The crude product was purified by recrystallization (m(CH_3OH): m(EtOAc) = 1∶1). The synthesis process is shown in Fig. 1.

(E)-4-Chloro-4'-ethoxystilbene(2a). Yield: 90.9%; melting point 175 to 177 ℃; IR (KBr, cm^{-1}) 3 018, 2 978, 1 603, 969, 835, 723; ^{1}H-NMR(400 MHz, DMSO) δ 7.58 to 7.53 (m, 4H), 7.42 (d, 2H), 7.23 (d, J = 16.0 Hz, 1H), 7.09 (d, J = 16.0 Hz, 1H), 6.94 (d, 2H), 4.05 (q, 2H), 1.34 (t, 3H).

(E)-4, 4'-dichlorostilbene (2b). Yield: 76.3%; melting point 74 to 76 ℃; IR (KBr, cm^{-1}) 3 060, 2 924, 963, 811, 740, 717; ^{1}H-NMR (400 MHz, DMSO) δ 7.86 to 7.83 (dd, 1H), 7.63 (d, 2H), 7.48 to 7.46 (dd, 1H), 7.43 (d, 2H), 7.44 (d, J = 16.4 Hz, 1H), 7.38 to 7.28 (m, 2H), 7.29 (d, J = 16.4 Hz, 1H).

1.3 X-ray crystallography

Colorless crystals of 2a (CCDC: 1573662) and 2b (CCDC: 1573663) were grown by slow evaporation from methanol and analyzed by ENRAF NONIUS CAD4 serial X-ray diffractometer equipped with a graphite-monochromatic MoKα radiation (λ = 0.071 073 nm) at 298 K. The OPTEP drawings and numbering scheme of crystals are exhibited in Fig. 2. The X-ray diffraction data and refinements are shown in Tab. 1. Crystogrpphic data is deposited in Cambridge Crystallographic Data Centre.

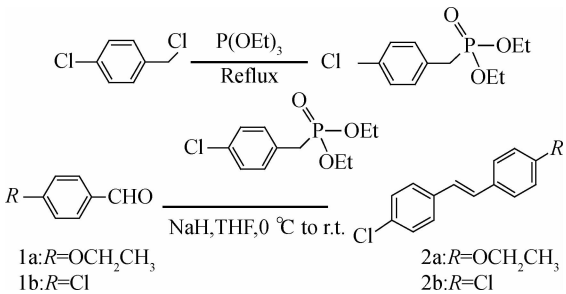

Fig. 1 The synthesis of 2a and 2b

Tab. 1 Crystal structures and refinement data of 2a and 2b

Parameter	Crystal of 2a	Crystal of 2b
Chemical formula	$C_{16}H_{15}ClO$	$C_{14}H_{10}Cl_2$
Formula weight	258.73	249.12
Crystal system	Orthorhombic	Monoclinic
Space group	Pna21	P21/C
Crystal density/ (g · cm^{-3})	1.259	1.380
a/nm	0.624 5	0.480 8
b/nm	0.742 3	1.027 3
c/nm	2.945 7	1.232 0
α/(°)	90	90
β/(°)	90	99.79
γ/(°)	90	90
V/nm^3	1.365 5	0.599 7
Formula units	4	4
Crystal size/ (mm × mm × mm)	0.30 × 0.30 × 0.10	0.20 × 0.10 × 0.10
T/K	293	293
Index range	$0 < h < 7$, $0 < k < 8$, $-35 < l < 35$	$0 < h < 5$, $0 < k < 12$, $-14 < l < 14$
F(000)	544	256
Completeness/%	100	100
R_1, $wR_2(I > 2\sigma(I))$	0.062 2, 0.122 1	0.052 5, 0.131 3
R_1, wR_2(all data)	0.146 4, 0.151 9	0.078 4, 0.146 6
Goodness of fit	1.004	1.003
θ_{min}, θ_{max}	1.38, 25.36	2.6, 25.36
CCDC deposit number	1 573 662	1 573 663

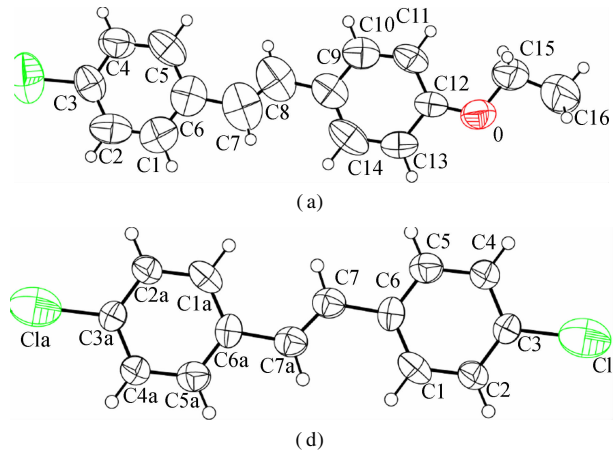

Fig. 2 OPTEP drawings and numbering schemes. (a) 2a; (b) 2b

2 Computational Methods

All the structures were optimized using B3LYP[8] method and 6-311 + + G (d, p)[9] basis set in Gaussian 09 software. B3LYP defines the exchange functional as a linear combination of Hatree-Fock, local and gradient-corrected exchange terms. 6-311G uses three sizes of contracted functions for each orbital-type. Meanwhile, the diffuse function can deal with molecules with lone pairs and polarized function allow orbitals to change size. After the optimization, the wave functions were acquired. Then, the Frontier molecular orbital and electrostatic potential are analyzed. The molecular Hirshfeld surface[10] of a crystal is constructed through partitioning the space into regions, which is determined by electron distribution. Normalized contact distance d_{norm} is used for mapping the surfaces and is calculated by the following equation:

$$d_{norm} = \frac{d_i - r^{vdw}}{r_i^{vdw}} + \frac{d_e - r_e^{vdw}}{r_e^{vdw}}$$

where d_i is the distance from Hirshfeld surface to the nearest nucleus internal; d_e is the distance from the surface to the nucleus external; r_i^{vdw} is the van der Waals radius of the atom of the nearest nucleus internal and r_e^{vdw} is the van der Waals radius of the atom of the nearest nucleus external. All of them are normalized by the van der Waals radius of the atom involved.

3 Results and Discussion

3.1 Crystal structure

Compound 2a was crystalized in the orthorhombic space group Pna21 and was found to adopt an E-configuration about its C═C bond, and C6, C7, C8 and C9 were almost in the same plane with a torsion angle of −179.29°. Compound 2b crystallized in the monoclinic space group P21/C and was also shown to have an E-configuration. The torsion angle of C6δ-C7δ-C7-C6 was

180°. The dihedral angles of two phenyl rings of 2a and 2b are 4.82° and 178°, respectively. Clearly, both compounds present a considerable coplanarity. Other relevant bond lengths and angles are presented in Tabs. 2 and 3.

Tab. 2 Selected bonding length and bonding angle determined by experiment and B3LYP of 2a

Bonding atoms	Bonding length/nm		Bonding atoms	Bonding angle/(°)	
	Experiment	B3LYP		Experiment	B3LYP
C1—C6	0.133 9	0.1405	C2—C3—Cl	119.74	119.74
C1—C2	0.132 9	0.139 1	Cl—C3—C4	119.55	119.55
C2—C3	0.1362	0.139 0	C5—C6—C7	125.71	123.77
C3—C4	0.133 3	0.139 4	C1—C6—C7	116.61	118.92
C3—Cl	0.174 5	0.175 9	C6—C7—C8	129.26	126.99
C4—C5	0.138 3	0.138 8	C7—C8—C9	127.94	127.41
C5—C6	0.143 8	0.140 7	C8—C9—C10	117.05	119.16
C6—C7	0.149 7	0.146 4	C8—C9—C14	125.30	123.84
C7—C8	0.120 6	0.134 7	C11—C12—O	126.39	124.93
C8—C9	0.1512	0.146 2	C13—C12—O	116.4	115.85
C9—C10	0.138 4	0.140 1	C12—O—C15	116.73	119.09
C9—C14	0.1362	0.141 0	O—C15—C16	107.03	107.72
C10—C11	0.136 8	0.139 4	Cl—C3—C2—C1	−179.59	180.00
C11—C12	0.136 6	0.139 7	Cl—C3—C4—C5	−178.72	−180.00
C12—C13	0.140 5	0.140 6	C5—C6—C7—C8	−5.76	0.34
C13—C14	0.140 4	0.138 2	C1—C6—C7—C8	173.18	−179.68
C12—O	0.132 6	0.136 2	C6—C7—C8—C9	−179.29	−179.98
O—C15	0.140 5	0.143 1	C7—C8—C9—C10	−167.43	−179.77
C15—C16	0.148 5	0.151 6	C7—C8—C9—C14	8.79	0.24
			C11—C12—O—C15	−2.02	0.01
			C13—C12—O—C15	178.85	−180.00
			C12—O—C15—C14	−172.64	−180.00

Tab. 3 Selected bonding length and bonding angle determined by experiment and B3LYP of 2b

Bonding atoms	Bonding length/nm		Bonding atoms	Bonding angle/(°)	
	Experiment	B3LYP		Experiment	B3LYP
C1—C2	0.139 8	0.138 8	Cl—C3—C4	119.39	119.72
C2—C3	0.136 7	0.139 4	Cl—C3—C2	119.61	119.52
C3—Cl	0.185 9	0.175 7	C5—C6—C7	117.64	118.83
C3—C4	0.138 5	0.139 0	C1—C6—C7	123.41	123.73
C4—C5	0.139 9	0.139 1	C6—C7—C7δ	124.78	127.10
C5—C6	0.136 6	0.140 5	Cl—C3—C4—C5	−178.90	180.00
C6—C1	0.139 2	0.140 7	Cl—C3—C2—C1	178.00	180.00
C6—C7	0.149 9	0.146 4	C5—C6—C7—C7δ	−1.76	180.00
C7—C7δ	0.129 0	0.134 6	C1—C6—C7—C7δ	178.14	0.00
			C6—C7—C7δ—C6δ	180.00	180.00

3.2 Hirshfeld surface and fingerprint plot

The molecular Hirshfeld surface and fingerprint plot can be utilized to provide information about three-dimensional intermolecular interactions in crystal. Three-dimensional maps are generated with d_{norm}, where the atoms make intermolecular contactors closer than van der Waals radii and the contacts are highlighted in red. White and blue indicate van der Waals contacts and ones longer than van der Walls contacts, respectively. Two-dimensional fingerprint plots are derived from the Hirshfeld surface, which summarizes the complex information according to the combination of d_e and d_i. Points on the plot are colored from green to blue with the increment of the contribution, while points with no contribution on the surface are left uncolored. The deep circular depressions on the surface represent hydrogen bonding contacts. Clearly, Fig. 3 shows strong interactions between O—H and Cl—H. π—π interactions are colored as red and blue triangles. Fig. 4 shows that there are considerable interactions between Cl—H. Two-dimensional fingerprint plots of 2a (see Fig. 5) shows four sharp spikes, which means that interaction appears between two adjacent molecules in the crystal structure. Points with no contribution to the surface are left uncoloured, points with small contribution are left green and points with more contribution are left blue. Reciprocal Cl—H and O—H offer contribution to the Hirshfeld surface with 16.3% and 4.3%, respectively. Therefore, it can be concluded that close contacts are mainly due to C—H—Cl and C—H—O hydrogen bonding.

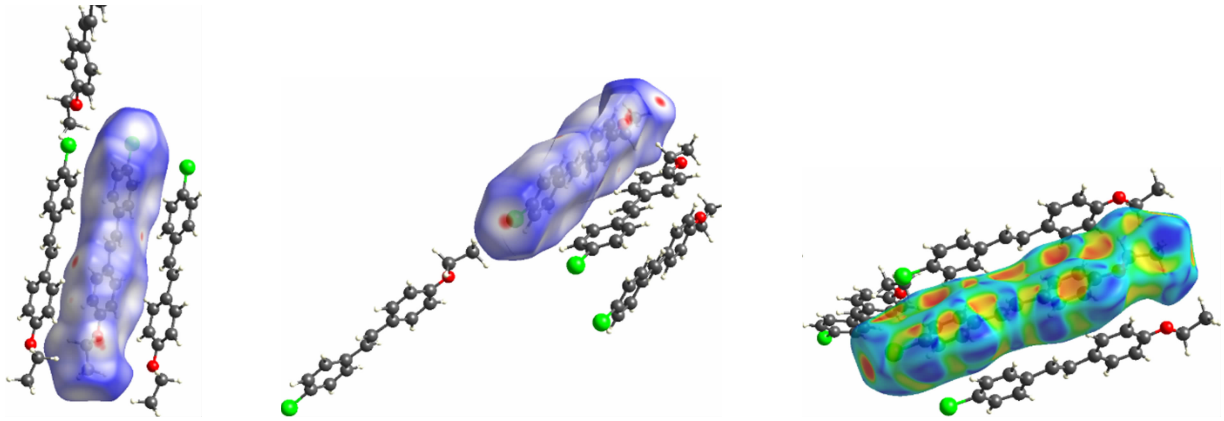

(a) (b) (c)

Fig. 3 Three-dimensional Hirshfeld maps of 2a. (a) Front view; (b) Back view; (c) Shape index

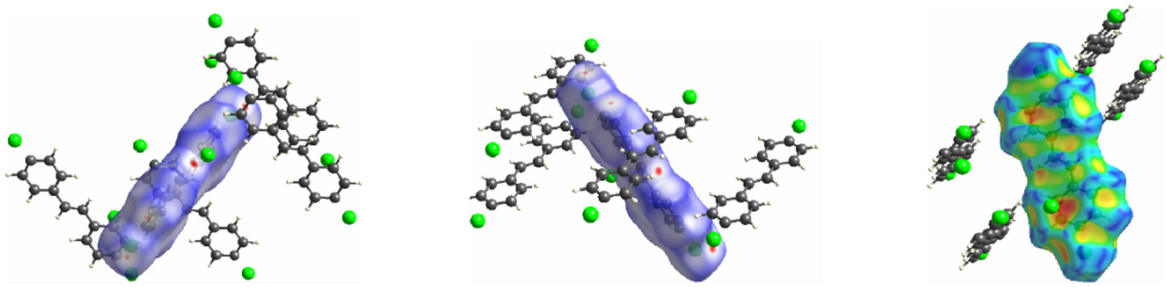

(a) (b) (c)

Fig. 4 Three-dimensional Hirshfeld maps of 2b. (a) Front view; (b) Back view; (c) Shape index

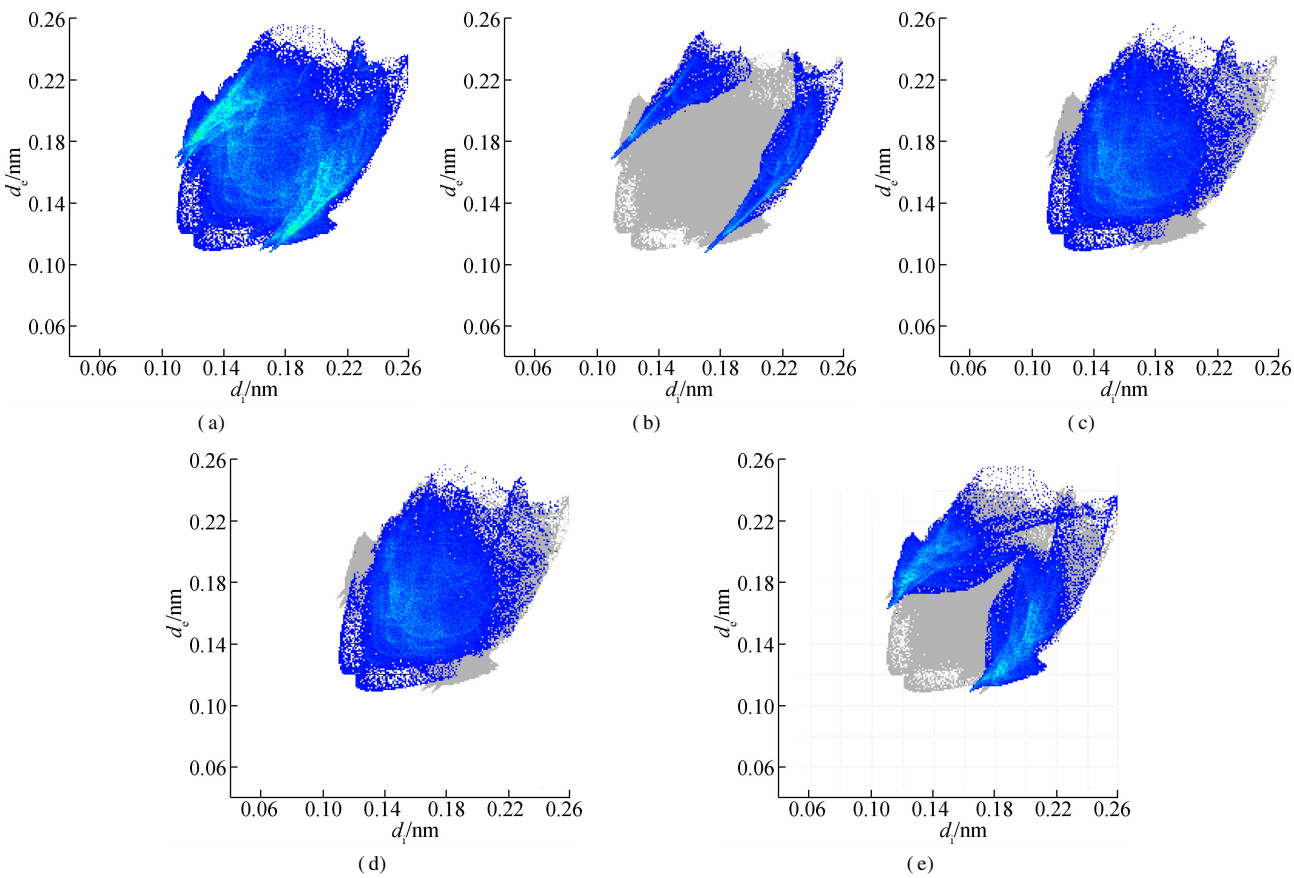

(a) (b) (c)

(d) (e)

Fig. 5 Two-dimensional fingerprint plots of 2a. (a) Full reciprocal; (b) Cl—H reciprocal; (c) O—H reciprocal; (d) H—H reciprocal; (e) C—H reciprocal

In addition, the reciprocal Cl—H of 2b (see Fig. 6) is 31.5%, which means that C—H—Cl hydrogen bonding contributed significantly to the Hirshfeld surface. Points with no contribution to the surface are left uncoloured, points with small contribution are left green and points with more contribution are left blue. As close contacts are mainly contributed by hydrogen bonding, C—H—Cl and C—H—O are the hydrogen bonding of 2a, and C—H—Cl is the hydrogen bonding of 2b. Thus, the results are consistent with single crystal structures.

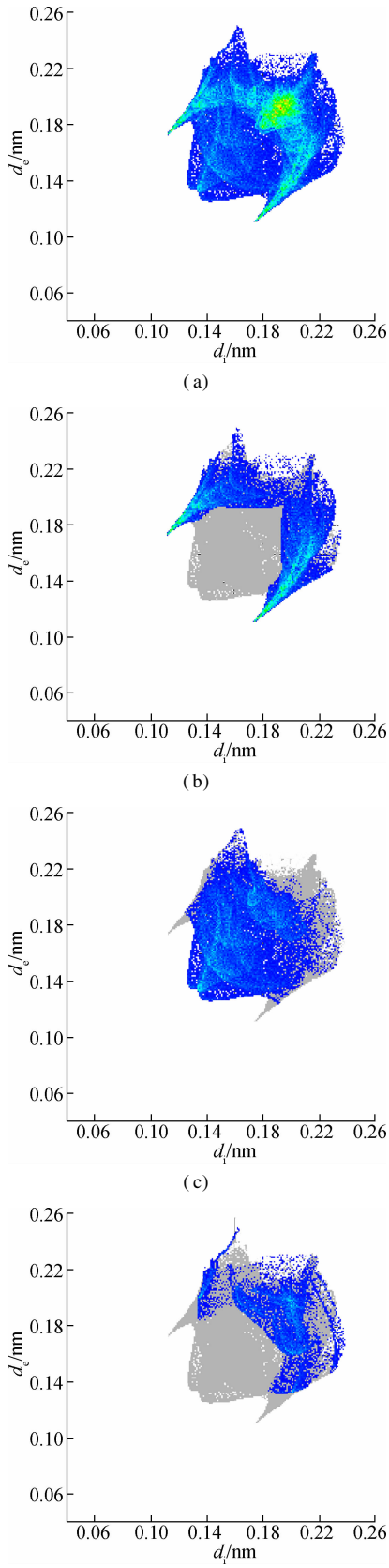

Fig. 6 Two-dimensional fingerprint plots of 2b. (a) Full reciprocal; (b) Cl—H reciprocal; (c) H—H reciprocal; (d) C—H reciprocal

3.3 Mulliken charge

Partial atom charge can be applied to analyze dipole moments, electronic structures, polarizabilities of molecules and chemical reactivity. Charge distributions of 2a and 2b are obtained by Mulliken population analysis, which computes charge by dividing orbital overlap evenly between the two atoms involved. The results are listed in Tabs. 4 and 5. The Cl atoms in the benzene ring of 2a and 2b have a high-positive charge of 0.460 and 0.492 a. u., respectively. Carbon atoms in C═C of 2a and 2b have a discrepant charge distribution due to the effect of ethyoxyl. C7 and C8 of 2a bear charges of 0.109 and −0.001 a. u. However, C7 of 2b has a charge of −0.004 a. u. The carbon atoms of two benzene ring of 2a bear different charges, C1—C6 of the benzene with Cl-substituted have charges in the range −1.085 to 0.371 a. u. In addition, C9—C14 of the benzene with ethyoxyl-substituted carry charges from −0.832 to 1.073 a. u. Carbon atoms C1—C6 of the benzene ring of 2b have charges in the range of −1.123 to −0.356 a. u. Different substituent groups do have considerable effect in the charge distribution of the benzene rings. However, the substituent effect decreases with the increase in distance.

Tab. 4 Mulliken charge of 2a

Atom	Charge/a. u.	Atom	Charge/a. u.	Atom	Charge/a. u.
C1	−0.168	C7	−0.179	C13	−0.229
C2	−0.221	C8	−0.150	C14	−0.161
C3	0.041	C9	−0.118	C15	−0.026
C4	−0.218	C10	−0.148	C16	−0.585
C5	−0.169	C11	−0.296	O	−0.552
C6	−0.078	C12	0.332	Cl	0.460

Tab. 5 Mulliken charge of 2b

Atom	Charge/a. u.	Atom	Charge/a. u.	Atom	Charge/a. u.
C1	−0.165	C7	−0.160	C2δ	−0.217
C2	−0.217	C7δ	−0.160	C1δ	−0.165
C3	−0.037	C6δ	0.083	Cl	0.492
C4	−0.221	C5δ	−0.164	Clδ	0.492
C5	−0.164	C4δ	−0.221		
C6	0.083	C3δ	−0.037		

3.4 Molecular electrostatic potential

Electrostatic potential (ESP) over molecular van der Waals surface is critical for understanding chemicalreactivities, charge density and delocalization. In-depth in-

vestigation of ESP can provide deeper understanding of the structure. Fig. 7 presents ESP-mapped molecular van der Waals surface of 2a and 2b. Molecular surface areas in ESP range, which are useful to quantitatively discuss the ESP distribution on the whole molecular surface of the products, as shown in Tab. 6. According to Fig. 7, lone pair of O atom leads to an ESP minima (−86.65 kJ/mol), which is the most negative on the van der Waals surface. Furthermore, the ESP minima located near the Cl atom have a value of −60.14 kJ/mol. As for 2b, the distribution of the minima is more symmetric, and for the two minima near two Cl atoms, which have a value of −47.38 kJ/mol. Each surface maximum corresponds to a hydrogen atom and the global maximum one of 2a and 2b are 91.96 and 108.90 kJ/mol, respectively. The surface areas of 2a and 2b are 3.1585 and 2.8184 nm^2, respectively. In Fig. 5, the negative values of ESP for 2a are concentrated between −54.37 and −35.55 kJ/mol (35.58%), while the positive values of ESP are concentrated in the range of 20.91 to 58.55 kJ/mol (40.00%). However, the distribution in 2b is symmetrical and moderate.

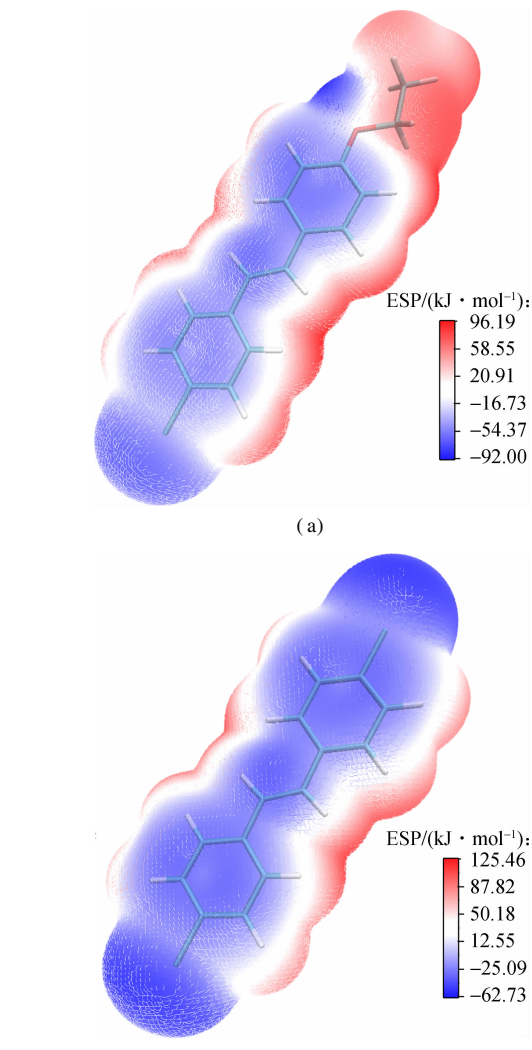

Fig. 7 Molecular electrostatic potential map. (a) 2a; (b) 2b

3.5 Frontier molecular orbitals

Frontier molecular orbitals have a critical role in determining the structures and properties of chemicals. The highest occupied molecular orbitals (HOMO) and lowest unoccupied molecularorbitals (LUMO) were calculated. LUMO+2, LUMO+1, LUMO, HOMO, HOMO−1 and HOMO−2 orbitals of 2a and 2b are presented in Fig. 8 and the relevant information is listed in Tab. 7. According to the results, the energy of HOMO and LUMO is −5.607 and −1.758 eV for 2a and −6.058 and −2.146 eV for 2b. Both products are stable as the energies of HOMO and LUMO, including neighboring orbitals, are all negative. HOMO and LUMO is known as the reference of electron donating and electron accepting potential. Higher $\Delta E_{\text{LUMO-HOMO}}$ means greater stability. $\Delta E_{\text{LUMO-HOMO}}$ of 2a and 2b are 3.85 and 3.91 eV, respectively.

Tab. 6 The distribution of molecular surface areas of 2a and 2b within different ESP ranges

ESP range of 2a/(kJ·mol^{-1})		Surface area/%	ESP range of 2b/(kJ·mol^{-1})		Surface area/%
Minimum	Maximum		Minimum	Maximum	
−92.00	−73.19	0.89	−62.73	−43.91	2.43
−73.19	−54.37	3.56	−43.91	−25.09	22.45
−54.37	−35.55	22.08	−25.09	−6.27	22.78
−35.55	−16.73	13.50	−6.27	12.55	12.17
−16.73	2.09	9.46	12.55	31.37	9.48
2.09	20.91	8.90	31.37	50.18	7.85
20.91	39.73	13.01	50.18	69.00	8.79
39.73	58.55	13.64	69.00	87.82	9.81
58.55	77.37	13.19	87.82	106.64	4.06
77.37	96.19	1.76	106.64	125.46	0.18

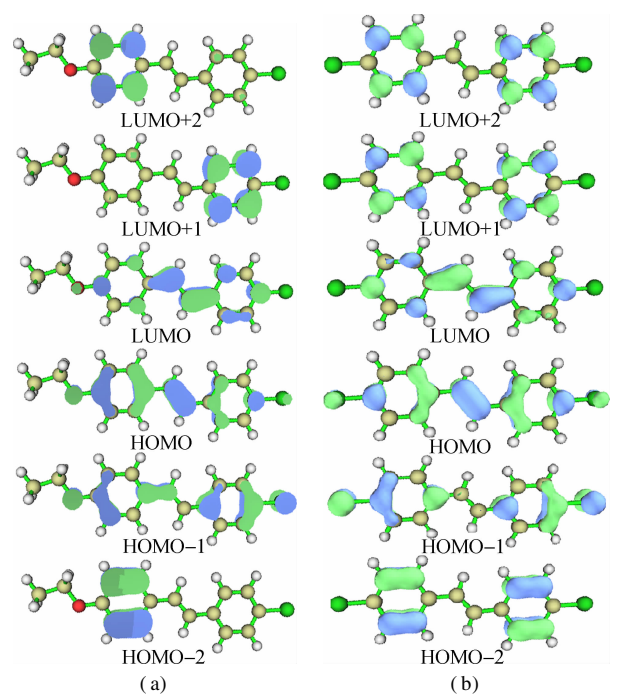

Fig. 8 Molecular frontier orbitals from HOMO−2 to LUMO+2. (a) 2a; (b) 2b

Tab. 7 The energies of molecular orbitals and the energy gap of HOMO and LUMO eV

Products	LUMO + 2	LUMO + 1	LUMO	HOMO	HOMO − 1	HOMO − 2	$\Delta E_{\text{LUMO - HOMO}}$
2a	−0.616	−0.761	−1.758	−5.607	−6.944	−7.268	3.85
2b	−0.934	−0.999	−2.146	−6.058	−7.382	−7.609	3.91

4 Conclusion

(E)-4-chloro-4'-ethoxystilbene (2a) and (E)-4, 4'-dichlorostilbene (2b) were synthesized and their single crystals were characterized. Compound 2a presented an orthorhombic space group Pna21 structure and 2b was found to be a monoclinic space group P21/c structure. Hirshfeld analyses revealed close O—H and Cl—H contacts in the crystal structure of 2a, while close Cl—H contacts existing in 2b. Electrostatic potential showed that O and Cl of 2a and Cl of 2b have most negative values. Therefore, they are more likely to undergo electrophilic attack. HOMO and LUMO orbitals of the benzene rings in both compounds are calculated according to the Frontier molecular orbitals and $\Delta E_{\text{LUMO-HOMO}}$ of 2b is higher than that of 2a.

References

[1] Menezes da Silva V H, de Lima Batista A P, Navarro O, et al. Theoretical study on selectivity trends in (N-heterocyclic carbene)-Pd catalyzed mizoroki-heck reactions: Exploring density functionals methods and molecular models [J]. *Journal of Computational Chemistry*, 2017, **38**(28): 2371 − 2377. DOI: 10.1002/jcc.24867. DOI: 10.1002/jcc.24867.

[2] Sirick A, Lednev S, Moskalenko I, et al. Kinetic features of chain initiation reactions during the oxidation of unsaturated compounds in media of different polarity [J]. *Reaction Kinetics Mechanisms and Catalysis,* 2015, **117**(2): 405 − 415. DOI: 10.1007/s11144 − 015 − 0957 − 6.

[3] Xu B, Fang H H, Chen F P, et al. Synthesis, characterization, two-photon absorption, and optical limiting properties of triphenylamine-based dendrimers [J]. *New Journal of Chemistry*, 2009, **33**(12): 2457. DOI: 10.1039/b9nj00393b.

[4] Xu H J, Zhao Y Q, Zhou X F. Palladium-catalyzed Heck reaction of aryl chlorides under mild conditions promoted by organic ionic bases[J]. *The Journal of Organic Chemistry*, 2011, **76** (19): 8036 − 8041. DOI: 10.1021/jo201196a.

[5] Li X B, Wang L, Zhang X Q, et al. A highly stereoselective synthesis of stilbenes under solvent-free conditions [J]. *Journal of Chemical Research*, 2010, **34**(9): 489 − 492. DOI: 10.3184/030823410x12814419570511.

[6] Thompson C M, Orellana M D, Lloyd S E, et al. Stereospecific synthesis of cis-stilbenes from benzaldehydes and phenylacetic acids via sequential Perkin condensation and decarboxylation [J]. *Tetrahedron Letters*, 2016, **57**(43): 4866 − 4868. DOI: 10.1016/j.tetlet.2016.09.069.

[7] Roman B I, de Coen L M, Mortier S T F C, et al. Design, synthesis and structure-activity relationships of some novel, highly potent anti-invasive (E)-and (Z)-stilbenes [J]. *Bioorganic & Medicinal Chemistry*, 2013, **21**(17): 5054 − 5063. DOI: 10.1016/j.bmc.2013.06.048.

[8] Hosna S, Janzen D E, Rzaigui M, et al. Synthesis, structural characterization, spectroscopic, thermal, dielectric and Hirshfeld surface analysis of 1-(2-methoxyphenyl) piperazinium chloranilate [J]. *Phase Transitions*, 2017, **91**(1): 15 − 25. DOI: 10.1080/01411594.2017.1350959.

[9] Becke A D. Density-functional thermochemistry. Ⅲ. The role of exact exchange [J]. *The Journal of Chemical Physics*, 1993, **98**(7): 5648 − 5652. DOI: 10.1063/1.464913.

[10] Lu T, Chen F W. Quantitative analysis of molecular surface based on improved Marching Tetrahedra algorithm [J]. *Journal of Molecular Graphics and Modelling*, 2012, **38**: 314 − 323. DOI: 10.1016/j.jmgm.2012.07.004.

(E)-4,4'-二氯二苯乙烯和(E)-4-氯-4'-乙氧基二苯乙烯的合成和计算

程金金　葛裕华

(东南大学化学化工学院, 南京 210096)

摘要:通过 Witting-Horner 反应合成化合物(E)-4,4'-二氯二苯乙烯(2a)和(E)-4-氯-4'-乙氧基二苯乙烯(2b). 采用溶剂挥发法制备 2a 和 2b 的晶体,并使用单晶衍射仪表征晶体结构. 分子结构分析表明 C═C 键为反式构型. 晶体 2a 为正交晶系,空间群为 Pna21;晶体 2b 为单斜晶系,空间群为 P21/c. 在 B3LYP/6-311 + + G(d,p)水平下优化 2a 和 2b 的电子结构. Hirshfeld 表面和指纹图表明,2a 和 2b 中有较强 O—H,Cl—H 氢键作用和 π—π 堆积作用. 分子静电势分析表明:2a 中的 O 和 Cl 原子及 2b 中的 Cl 原子有能量极小值,在反应过程中容易被亲电试剂进攻. 前线分子轨道分析表明,2a 和 2b 的 $\Delta E_{\text{LUMO-HOMO}}$ 分别为 3.85 和 3.91 eV.

关键词:二苯乙烯;晶体结构;密度泛函理论;合成

中图分类号:O621